

Floquet engineering of strongly driven excitons in monolayer tungsten disulfide

Received: 28 May 2022

Accepted: 20 October 2022

Published online: 5 January 2023

 Check for updates

Yuki Kobayashi  , Christian Heide  , Amalya C. Johnson  , Vishal Tiwari⁴, Fang Liu  , David A. Reis  , Tony F. Heinz^{1,2,6} & Shambhu Ghimire¹ 

Interactions of quantum materials with strong laser fields can induce exotic non-equilibrium electronic states^{1–6}. Monolayer transition metal dichalcogenides, a new class of direct-gap semiconductors with prominent quantum confinement⁷, offer exceptional opportunities for the Floquet engineering of excitons, which are quasiparticle electron–hole correlated states⁸. Strong-field driving has the potential to achieve enhanced control of the electronic band structure and thus the possibility of opening a new realm of exciton light–matter interactions. However, a full characterization of strong-field driven exciton dynamics^{4,9} has been difficult. Here we use mid-infrared laser pulses below the optical bandgap to excite monolayer tungsten disulfide and demonstrate strong-field light dressing of excitons in excess of a hundred millielectronvolts. Our high-sensitivity transient absorption spectroscopy further reveals the formation of a virtual absorption feature below the 1s-exciton resonance, which we assign to a light-dressed sideband from the dark 2p-exciton state. Quantum-mechanical simulations substantiate the experimental results and enable us to retrieve real-space movies of the exciton dynamics. This study advances our understanding of the exciton dynamics in the strong-field regime, showing the possibility of harnessing ultrafast, strong-field phenomena in device applications of two-dimensional materials.

Laser-field manipulation of electronic band structures is at the frontier of quantum-materials research⁵. In particular, monolayer transition metal dichalcogenides exhibit remarkable excitonic properties as a result of their atomic-scale thickness⁷, and recent spectroscopic studies have shown their promising potential for novel optoelectronic devices^{10–19}. One of the common approaches is to drive the interband transition coherently by a near-resonant visible pulse and to induce an a.c.-Stark shift to the exciton resonance^{10–12}. Another possible, yet largely unexplored, approach is to drive excitons with a strong laser field, thereby directly imparting momentum from the oscillating laser

field to the electron–hole pairs. This limit of light–matter interactions is known as the strong-field regime²⁰, in which unique laser-induced phenomena occur, such as high-harmonic generation²¹, high-order sideband generation^{4,9}, subcycle dynamic Franz–Keldysh effects²² and predicted control of topological properties²³.

To describe the strong-field regime of exciton dynamics, it is useful to consider the critical-field strength (F_c) that is required to break apart an exciton into a free electron–hole pair. At the dipole limit, the critical-field strength can be approximated by comparing the exciton binding energy (E_b) and Bohr radius (a_B), with $F_c = \frac{E_b}{e a_B}$. Typical param-

¹Stanford PULSE Institute, SLAC National Accelerator Laboratory, Menlo Park, CA, USA. ²Department of Applied Physics, Stanford University, Stanford, CA, USA. ³Department of Materials Science and Engineering, Stanford University, Stanford, CA, USA. ⁴Department of Chemistry, University of Rochester, Rochester, NY, USA. ⁵Department of Chemistry, Stanford University, Stanford, CA, USA. ⁶Department of Photon Science, Stanford University, Stanford, CA, USA. ⁷These authors contributed equally: Yuki Kobayashi, Christian Heide.  e-mail: ykb@stanford.edu; shambhu@stanford.edu

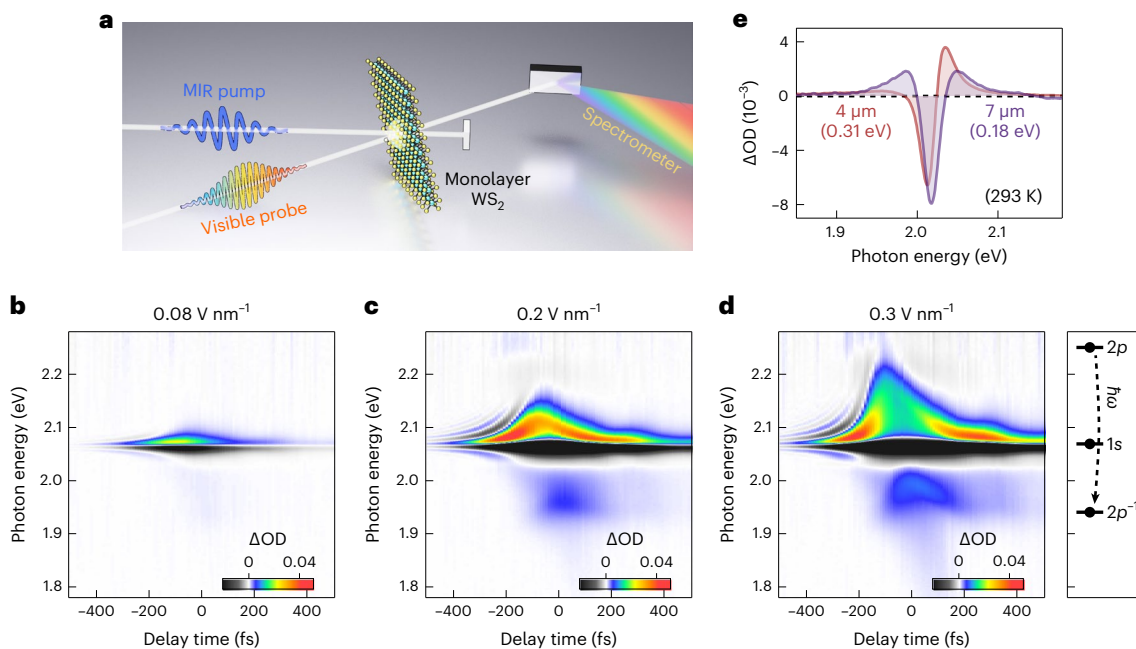


Fig. 1 | Transient absorption spectra of strongly driven excitons in monolayer

WS₂. **a**, Outline of the experiment. A mid-infrared (MIR) pump pulse drives coherent exciton dynamics in monolayer WS₂, and a visible probe pulse records the light-dressing effects in its transmission spectrum. **b–d**, Transient absorption spectra (ΔOD) of monolayer WS₂ at 77 K driven by a 4 μm mid-infrared field. The positive delay corresponds to the visible probe pulse following the mid-infrared pump pulse. The presence of a positive spectral chirp in the visible spectrum causes an overall tilt of the transient absorption signals, but this does not affect our main discussion. At a field strength of 0.08 V nm^{-1} (**b**), the light-dressing effect induces a blue shift of the 1s-exciton signal via the a.c.-Stark shift. As the intensity increases to 0.2 V nm^{-1} (**c**), the a.c.-Stark shift grows, and a new

absorption feature emerges below the 1s-exciton resonance, which corresponds to a light-dressed sideband of the 2p-exciton state, or the 2p⁻¹-exciton state. At the highest intensity of 0.3 V nm^{-1} (**d**), substantial blue shifts are observed both for the 1s- and 2p⁻¹-exciton states. The energy diagram on the right shows the estimated energies of the unperturbed light-dressed exciton states. **e**, Dependence of the a.c.-Stark shift on the pump wavelength at the 1s-exciton resonance at zero delay time. The asymmetric blue shift under 4 μm driving changes to a symmetric response under 7 μm driving, which yields an estimated 1s–2p transition energy of 0.18 eV. These measurements were performed at room temperature.

eters of $E_b \approx 300$ meV and $a_b \approx 1$ nm (ref. 24) yield the critical-field strength of approximately 0.3 V nm^{-1} (laser intensity of 12 GW cm^{-2}). Cunningham et al. reported the largest a.c.-Stark shift of 32 meV with a visible excitation, but the applied field strength was less than 0.03 V nm^{-1} (less than 0.14 GW cm^{-2})¹⁴.

Driving and probing strong-field processes in two-dimensional materials poses several experimental challenges. First, sample damage may occur as a result of absorption and carrier generation by irradiation with an intense laser. Second, light-dressing effects are coherent processes that are induced only during the laser excitation. Therefore, it is desirable to use a coherent optical probe, rather than a process such as photoluminescence, so as to be sensitive to the phase-coherent response of the material. Finally, experimental signatures of the field-driven dynamics, particularly those from exciton states, are yet to be established.

Here we overcome these challenges and demonstrate strong-field control of exciton states in monolayer tungsten disulfide (WS₂). Our main experimental findings include an anomalously large energy shift to the 1s-exciton resonance, and the emergence of a light-dressed Floquet sideband from the 2p-exciton state. Experimentally, a 200 fs mid-infrared pulse of 4.0 μm wavelength (photon energy of 0.31 eV, frequency of 75 THz) is used to excite monolayer WS₂ (Fig. 1a). The small photon energy of the mid-infrared pulse allows us to reach a field strength of 0.3 V nm^{-1} without damaging the sample, whereas light-dressing effects are induced by coherently driving the internal resonance of the exciton states^{15,25}. Such an intense mid-infrared pulse is produced by difference-frequency generation in a gallium–selenide crystal by using the output of a high-power optical-parametric amplification system. We used optical transient absorption spectroscopy as

a probe, with a broadband visible pulse encoding the excitonic energy structure in its transmission spectrum. The differential absorption (ΔOD) is obtained by taking the pump-on (I_{on}) and pump-off (I_{off}) spectra at a controlled delay time t to determine $\Delta\text{OD} = -\log(I_{\text{on}}/I_{\text{off}})$. A positive ΔOD corresponds to induced absorption, whereas a negative ΔOD corresponds to reduced absorption. Sensitivity to weak changes in absorption is achieved by means of single-shot detection; accumulation of 30,000 laser shots leads to the detection sensitivity of 3×10^{-5} . A high-quality, millimetre-scale sample of monolayer WS₂ was prepared by the gold-tape exfoliation method^{26,27}. The sample was probed in a vacuum cryostat at a temperature of 77 K, unless otherwise noted.

Transient absorption spectra of monolayer WS₂ under 4 μm driving are shown in Fig. 1b–d. At a lower mid-infrared intensity (Fig. 1b; 0.08 V nm^{-1}), the 1s-exciton signal at 2.07 eV shows a blue shift. This asymmetric behaviour cannot be explained by a simple peak broadening¹⁷, demonstrating that the underlying exciton light–matter interactions are coherent in nature. Additional measurements were carried out at alternate mid-infrared wavelengths. For a 7 μm driving field (photon energy of 0.18 eV), the transient absorption signal is found to be symmetric (Fig. 1e). The symmetric change indicates that the 7 μm radiation is nearly resonant with the intra-excitonic transition¹⁵, thus yielding an estimated 1s–2p transition energy of 0.18 eV.

At a higher intensity (Fig. 1c, 0.2 V nm^{-1}), a large (approximately 40 meV) blue shift is observed at the 1s-exciton resonance. More importantly, a new absorption feature emerges below the 1s-exciton resonance, which we assign to a single-photon-dressed Floquet sideband of the 2p-exciton state or the 2p⁻¹-exciton state. The original 2p-exciton state is dipole forbidden from the ground state and does not directly contribute to the absorption spectra²⁸. Single-photon dressing,

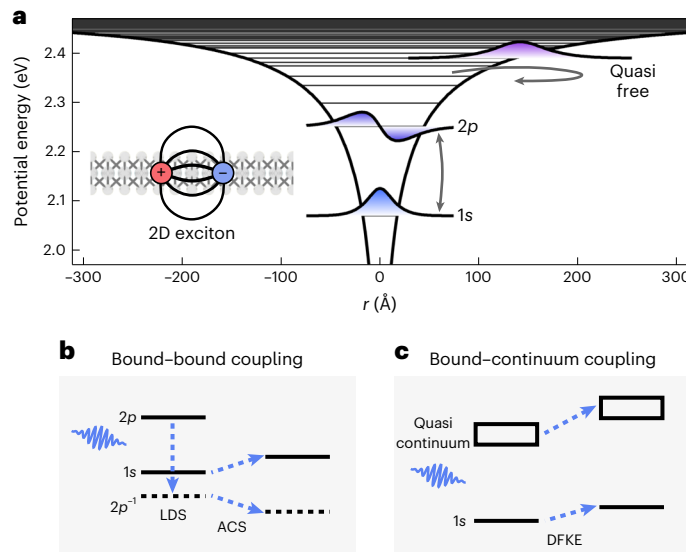


Fig. 2 | Light-dressing mechanisms of strongly driven excitons. **a**, An effective two-dimensional potential for excitons and the associated energy levels. An external laser field can excite internal resonances of excitons, such as the $1s\text{--}2p$ transition, and drive the exciton wavepacket into the quasifree region of the potential. **b,c**, Schematic illustration of the light-dressing effects. In the bound–bound coupling case (**b**), an external laser field can create light-dressed sidebands (LDS) and the mixing between the light-dressed states induces the a.c.–Stark shift (ACS). In the bound–continuum coupling case (**c**), excitons can gain kinetic energy from the external laser field in the quasifree region, and the renormalization of the energy levels results in the dynamic Franz–Keldysh effect (DFKE).

however, can create a replica of the $2p$ -exciton state that has the opposite parity. Hybridization between the bright $1s$ -exciton state can impart optical strength under a moderate driving intensity, thus creating a new virtual state that is present only during the mid-infrared driving. Note that two-photon-dressed Floquet sidebands of the $1s$ -exciton state are also possible, but the hybridization with the original $1s$ -exciton state is weaker owing to the larger energy separation.

There are three additional noteworthy features (Fig. 1c). One feature is hyperbolic sidebands that appear around the $1s$ -exciton signal at the negative delays (that is, the visible probe pulse arriving first). This can be understood as the result of perturbation of the free-induction decay at the $1s$ -exciton resonance by the strong mid-infrared field, which is manifested as a change in the lineshape from Lorentzian to a sinc function²⁹. Another observation is that much longer delays (> 500 fs) do not show significant absorption, such as with $\Delta OD < 0.8 \times 10^{-3}$ at 3,000 fs (Supplementary Fig. 2c), which indicates that direct multiphoton generation of carriers by the strong mid-infrared laser field can be neglected. The last feature is the apparent transient response at delay times around 300 fs. This may arise from a satellite structure in the temporal profile of the broadband mid-infrared pulse.

As the mid-infrared drive intensity increases to 0.3 V nm^{-1} for a laser fluence of approximately 2 mJ cm^{-2} (Fig. 1d), the blue shift of the $1s$ -exciton resonance is accompanied by peak broadening, which is indicative of exciton ionization. We also observe that the $2p^1$ -exciton feature undergoes a large (approximately 40 meV) blue shift. As we explain below, this is an unexpected result within the conventional two-level picture; if the a.c.–Stark shift causes a blue shift to the $1s$ -exciton state, the paired $2p^1$ -exciton state should experience a red shift of the same magnitude.

We now proceed to a theoretical analysis of the experimental results. Our primary interest lies in finding optical signatures of the field-driven dynamics of excitons. The mechanisms of the mid-infrared light dressing are illustrated in Fig. 2a–c. When the excitation is limited to the lower bound states, such as the $1s$ - and $2p$ -exciton states, the

light-dressing effect can be understood within the Floquet theory (Fig. 2b)^{30,31}. The external laser field creates replicas of the exciton states that are evenly spaced by the driving-photon energy, and hybridization between the neighbouring states leads to a.c.–Stark shifts¹⁵. Going beyond a picture involving the only lower bound exciton states, a strong applied field can, however, lead to exciton wavepackets that are driven out of the bound potential to the quasifree region (Fig. 2c). The excitons in the asymptote can gain substantial kinetic energy from the oscillating laser field, which leads to renormalization of energy levels (that is, the dynamic Franz–Keldysh effect)^{32,33}. In the case of a parabolic band (that is, quasifree electrons), the renormalization results in a universal blue shift of the energy structure by the amount equal to the ponderomotive energy³⁴.

We simulate transient absorption spectra of the strongly driven excitons with two models. In the first model, the exciton light–matter interactions are fully considered, including the bound–bound coupling, bound–continuum coupling and ionization. This is achieved by numerically solving the time-dependent Schrödinger equation (TDSE) for an exciton wavepacket in the non-hydrogenic two-dimensional Rytova–Keldysh potential^{24,35},

$$V(r) = -\frac{\pi e^2}{2r_0} \left[H_0\left(\frac{r}{r_0}\right) - Y_0\left(\frac{r}{r_0}\right) \right], \quad (1)$$

where H_0 and Y_0 are Struve and Bessel functions and r_0 is the screening length of Coulomb attraction in monolayer WS₂ (Fig. 2a). The reduced mass of the exciton is fixed at $\mu = 0.16 m_0$ (ref. 36), and the free parameter of the screening length is chosen to be $r_0 = 50 \text{ \AA}$ so that the experimental $1s\text{--}2p$ transition energy of 0.18 eV is reproduced. The other model uses a minimum discrete system that consists only of the ground, $1s$ - and $2p$ -exciton states. In this case, the mid-infrared field can drive only one bound–bound coupling, that is, the $1s\text{--}2p$ transition, and the exciton dynamics in the quasifree region are excluded. In both models, the absorption cross-section of the exciton wavepacket is calculated as $\sigma(\omega) \propto \omega \text{Im} \left[\frac{\tilde{d}(\omega)}{\tilde{E}(\omega)} \right]$, where $\tilde{d}(\omega)$ and $\tilde{E}(\omega)$ are the Fourier-transformed optical dipole moment and laser electric field, respectively (see Methods for more details)³⁷.

Figure 3 shows the comparison of the experimental (Fig. 3a) and simulated (Fig. 3b,c) transient absorption spectra at various mid-infrared intensities. To account for the visible spectral chirp in the experiments, the transient absorption signals below and above the $1s$ -exciton resonance are measured at 60 fs and -60 fs, respectively. The peak energies are evaluated for the ΔOD plots; see Supplementary Fig. 5 for the analysis of the absorption (OD) plots. In the low-intensity case at 0.05 V nm^{-1} (Fig. 3d), the a.c.–Stark shift is the main feature of the transient absorption signals, and both models reproduce the experimental result. In the high-intensity case at 0.25 V nm^{-1} (Fig. 3d), the two-dimensional time-dependent Schrödinger equation (2D-TDSE) method captures the anomalously large blue shift in the $1s$ -exciton signal as well as the emergence of the light-dressed $2p^1$ -exciton state. In contrast, the $1s\text{--}2p$ model exhibits a poor agreement with experiment; the energy of the $1s$ - and $2p^1$ -exciton signals are underestimated by approximately 30 meV and approximately 80 meV, respectively. Overall, the 2D-TDSE method successfully reproduces the $1s$ - and $2p^1$ -exciton signals throughout the intensity regime measured in the experiments, whereas the $1s\text{--}2p$ model works only at the lower field strengths (Fig. 3e). The contrast between the two models originates from the fact that the 2D-TDSE method fully considers the bound–bound and bound–continuum couplings that are expressed within the grid space ($r \leq 300 \text{ \AA}$), whereas the $1s\text{--}2p$ model is restricted to the single bound–bound coupling.

The good agreement between the experiments and the 2D-TDSE simulations further allows us to obtain real-space pictures of the strongly driven excitons (Fig. 4). Here, the initial wavepacket is

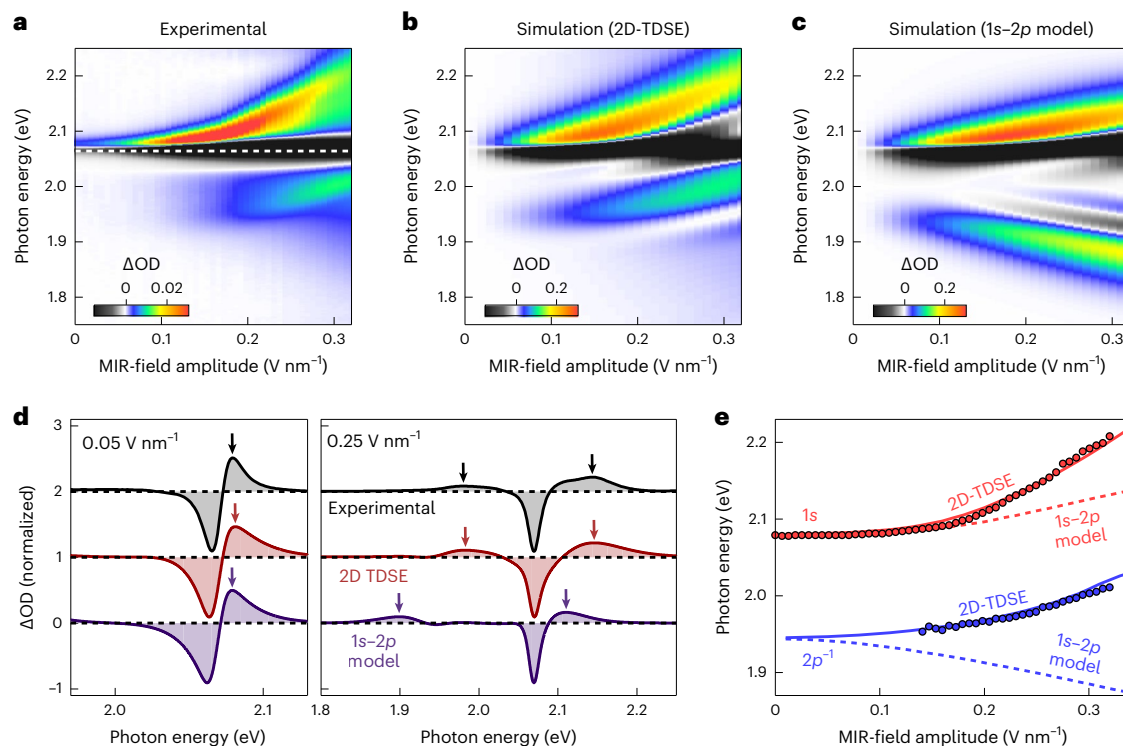


Fig. 3 | Optical signatures of the field-driven exciton dynamics. **a–c**, Transient absorption spectra (ΔOD) of monolayer WS_2 driven by a $4 \mu\text{m}$ mid-infrared field at various intensities. The experimental transient absorption spectra (**a**) are obtained by combining the results at -60 fs and 60 fs delay times for above and below the 1s-exciton resonance, respectively, to account for the positive chirp in the visible spectrum. The experimental results are compared to the

simulation results obtained by the 2D-TDSE method (**b**) and the 1s-2p model (**c**). **d**, Comparison of the transient absorption spectra at low (0.05 V nm^{-1}) and high (0.25 V nm^{-1}) mid-infrared field strengths. The arrows indicate the peak energies of the 1s- and 2p⁻¹-exciton states. **e**, Summary of the experimental and simulated peak energies for the 1s- and 2p⁻¹-exciton states.

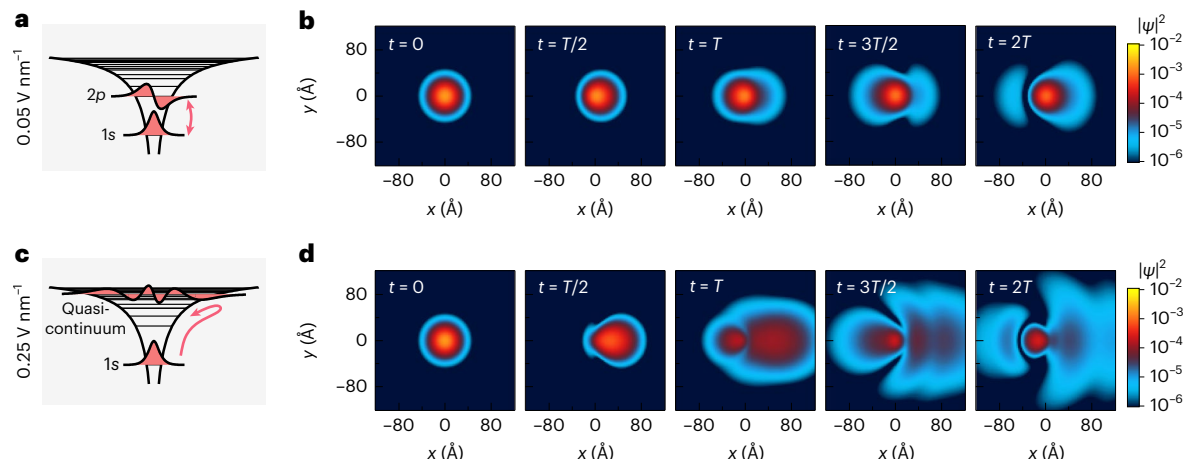


Fig. 4 | Snapshots of the exciton wavepacket. **a**, Schematic of the exciton dynamics in a low-intensity case (0.05 V nm^{-1}). **b**, Snapshots of the exciton wavepacket (squared probability distribution) obtained in 2D-TDSE simulations. The wavepacket remains localized at the potential centre, and it exhibits only one node after two cycles ($t = 2T$) of the mid-infrared excitation. This shows that the excitation is limited to the 2p-exciton state. **c**, Schematic of the exciton

dynamics in a high-intensity case (0.25 V nm^{-1}). **d**, Here the strong mid-infrared field drives the exciton wavepacket out of the bound potential into the quasifree region within a single cycle. The wavepacket is no longer localized at the potential centre, and the multiple nodes appearing in the snapshots arise from the interference between the excited-state quasicontinuum.

assumed to be the 1s-exciton state launched by the visible pulse at $t = 0$, and the mid-infrared driving field is a sine pulse (that is, the electric field is zero at $t = 0$). In the low-intensity case at 0.05 V nm^{-1} (Fig. 4a,b), the exciton wavepacket remains localized around the potential centre. After two cycles ($t = 2T$), the exciton wavepacket exhibits only one node, which shows that the excitation is limited to the 2p-exciton state. In the high-intensity case at 0.25 V nm^{-1} (Fig. 4c,d),

the centre-of-mass of the wavepacket moves by approximately 30 \AA only after a half cycle ($t = T/2$). Multiple nodal features emerge at later times, which originate from the interference between the excited-state quasicontinuum. Note that a certain portion of the population remains at the potential centre, which shows that we are in the regime where both the bound–bound coupling (that is, the a.c.-Stark shift) and the bound–continuum coupling (that is, the dynamic Franz–Keldysh

effect) are relevant. These observations, in combination with the results in Fig. 3, establish the role of the field-driven dynamics of excitons under strong mid-infrared driving.

In conclusion, we have investigated the strong-field regime of the exciton dynamics in monolayer WS₂ by using an intense mid-infrared pump in a transient absorption configuration. We characterized an anomalously large (approximately 140 meV) blue shift in the 1s-exciton resonance and a completely new light-dressed sideband originating from the optically dark 2p-exciton state. We reproduced the experimental results by solving the time-dependent Schrödinger equation in a two-dimensional Rytova–Keldysh potential, which subsequently allowed us to reconstruct the subcycle evolution of the exciton wavepackets. Our real-space model provides a natural extension of the basic two-level framework, which may be of use in future exciton experiments. The combined results of the experiment and theory extend the knowledge of exciton light–matter interactions beyond the perturbative a.c.–Stark shift to the field-driven regime, revealing efficient new approaches to manipulate monolayer excitons. Our study also shows that even at the critical-field strength of ionization, the exciton picture still holds for the mid-infrared excitations. The oscillating mid-infrared field imparts substantial momentum to the excitons, while still maintaining the electron–hole overlap. Previously, subcycle control of electron motion was studied for atomic systems^{38,39}. Now that the applicability of the same concept has been established for two-dimensional materials, it might be possible to trigger and control the motion of excitons at the fundamental time scale of the driving-laser fields. For example, a half cycle of the 4 μm excitation corresponds to a period of 6.7 fs (150 THz). This will open the path towards atomically thin electroabsorption modulators with operation frequencies approaching the petahertz regime⁴⁰. Our results also suggest that strongly driven excitons could affect the high-harmonic generation process in monolayer transition metal dichalcogenides, in which enhanced per-layer efficiency has been reported compared to the bulk⁴¹.

Online content

Any methods, additional references, Nature Portfolio reporting summaries, source data, extended data, supplementary information, acknowledgements, peer review information; details of author contributions and competing interests; and statements of data and code availability are available at <https://doi.org/10.1038/s41567-022-01849-9>.

References

- Wagner, M. et al. Observation of the intraexciton autler–townes effect in GaAs/AlGaAs semiconductor quantum wells. *Phys. Rev. Lett.* **105**, 167401 (2010).
- Teich, M. et al. Systematic investigation of terahertz-induced excitonic Rabi splitting. *Phys. Rev. B* **89**, 115311 (2014).
- Uchida, K. et al. Time-resolved observation of coherent excitonic nonlinear response with a table-top narrowband THz pulse wave. *Appl. Phys. Lett.* **107**, 221106 (2015).
- Langer, F. et al. Lightwave valleytronics in a monolayer of tungsten diselenide. *Nature* **557**, 76–80 (2018).
- McIver, J. W. et al. Light-induced anomalous hall effect in graphene. *Nat. Phys.* **16**, 38–41 (2020).
- Baykusheva, D. et al. All-optical probe of three-dimensional topological insulators based on high-harmonic generation by circularly polarized laser fields. *Nano Lett.* **21**, 8970–8978 (2021).
- Mak, K. F., Lee, C., Hone, J., Shan, J. & Heinz, T. F. Atomically thin MoS₂: a new direct-gap semiconductor. *Phys. Rev. Lett.* **105**, 136805 (2010).
- Wang, G. et al. Colloquium: excitons in atomically thin transition metal dichalcogenides. *Rev. Mod. Phys.* **90**, 021001 (2018).
- Zaks, B., Liu, R. B. & Sherwin, M. S. Experimental observation of electron–hole recollisions. *Nature* **483**, 580–583 (2012).
- Kim, J. et al. Ultrafast generation of pseudo-magnetic field for valley excitons in WSe₂ monolayers. *Science* **346**, 1205–1208 (2014).
- Sie, E. J. et al. Valley-selective optical stark effect in monolayer WS₂. *Nat. Mater.* **14**, 290–294 (2015).
- Ye, Z., Sun, D. & Heinz, T. F. Optical manipulation of valley pseudospin. *Nat. Phys.* **13**, 26–29 (2017).
- Yong, C.-K. et al. Biexcitonic optical stark effects in monolayer molybdenum diselenide. *Nat. Phys.* **14**, 1092–1096 (2018).
- Cunningham, P. D., Hanbicki, A. T., Reinecke, T. L., McCreary, K. M. & Jonker, B. T. Resonant optical stark effect in monolayer WS₂. *Nat. Commun.* **10**, 5539 (2019).
- Yong, C.-K. et al. Valley-dependent exciton fine structure and autler–townes doublets from berry phases in monolayer MoSe₂. *Nat. Mater.* **18**, 1065–1070 (2019).
- Morrow, D. J. et al. Quantum interference between the optical stark effect and resonant harmonic generation in WS₂. *Phys. Rev. B* **102**, 161401 (2020).
- Shi, J. et al. Room temperature terahertz electroabsorption modulation by excitons in monolayer transition metal dichalcogenides. *Nano Lett.* **20**, 5214–5220 (2020).
- Earl, S. K. et al. Coherent dynamics of floquet–bloch states in monolayer WS₂ reveals fast adiabatic switching. *Phys. Rev. B* **104**, L060303 (2021).
- LaMountain, T. et al. Valley-selective optical stark effect of exciton-polaritons in a monolayer semiconductor. *Nat. Commun.* **12**, 4530 (2021).
- Brabec, T. & Krausz, F. Intense few-cycle laser fields: frontiers of nonlinear optics. *Rev. Mod. Phys.* **72**, 545 (2000).
- Ghimire, S. et al. Observation of high-order harmonic generation in a bulk crystal. *Nat. Phys.* **7**, 138–141 (2011).
- Lucchini, M. et al. Attosecond dynamical Franz–Keldysh effect in polycrystalline diamond. *Science* **353**, 916–919 (2016).
- Silva, R. E. F., Jiménez-Galán, Á., Amorim, B., Smirnova, O. & Ivanov, M. Topological strong-field physics on sub-laser-cycle timescale. *Nat. Photon.* **13**, 849–854 (2019).
- Chernikov, A. et al. Exciton binding energy and nonhydrogenic rydberg series in monolayer WS₂. *Phys. Rev. Lett.* **113**, 076802 (2014).
- Poellmann, C. et al. Resonant internal quantum transitions and femtosecond radiative decay of excitons in monolayer WSe₂. *Nat. Mater.* **14**, 889–893 (2015).
- Ajai, O. A. et al. Approaching the intrinsic photoluminescence linewidth in transition metal dichalcogenide monolayers. *2D Mater.* **4**, 031011 (2017).
- Liu, F. et al. Disassembling 2D van der Waals crystals into macroscopic monolayers and reassembling into artificial lattices. *Science* **367**, 903–906 (2020).
- Ye, Z. et al. Probing excitonic dark states in single-layer tungsten disulphide. *Nature* **513**, 214–218 (2014).
- Lindberg, M. & Koch, S. W. Transient oscillations and dynamic stark effect in semiconductors. *Phys. Rev. B* **38**, 7607 (1988).
- Shirley, J. H. Solution of the Schrödinger equation with a Hamiltonian periodic in time. *Phys. Rev.* **138**, B979 (1965).
- Sambe, H. Steady states and quasienergies of a quantum-mechanical system in an oscillating field. *Phys. Rev. A* **7**, 2203 (1973).
- Jauho, A. P. & Johnsen, K. Dynamical Franz–Keldysh effect. *Phys. Rev. Lett.* **76**, 4576 (1996).
- Nordstrom, K. B. et al. Excitonic dynamical Franz–Keldysh effect. *Phys. Rev. Lett.* **81**, 457 (1998).
- Tsuji, N., Oka, T. & Aoki, H. Correlated electron systems periodically driven out of equilibrium: Floquet+DMFT formalism. *Phys. Rev. B* **78**, 235124 (2008).

35. Keldysh, L. V. Coulomb interaction in thin semiconductor and semimetal films. *JETP Lett.* **29**, 716–719 (1979).
36. Berkelbach, T. C., Hybertsen, M. S. & Reichman, D. R. Theory of neutral and charged excitons in monolayer transition metal dichalcogenides. *Phys. Rev. B* **88**, 045318 (2013).
37. Wu, M., Chen, S., Camp, S., Schafer, K. J. & Gaarde, M. B. Theory of strong-field attosecond transient absorption. *J. Phys. B: At. Mol. Opt. Phys.* **49**, 062003 (2016).
38. Chini, M. et al. Sub-cycle oscillations in virtual states brought to light. *Sci. Rep.* **3**, 1105 (2013).
39. Ott, C. et al. Reconstruction and control of a time-dependent two-electron wave packet. *Nature* **516**, 374–378 (2014).
40. Kruchinin, S. Y., Krausz, F. & Yakovlev, V. S. Colloquium: strong-field phenomena in periodic systems. *Rev. Mod. Phys.* **90**, 021002 (2018).
41. Liu, H. et al. High-harmonic generation from an atomically thin semiconductor. *Nat. Phys.* **13**, 262–265 (2017).

Publisher's note Springer Nature remains neutral with regard to jurisdictional claims in published maps and institutional affiliations.

Springer Nature or its licensor (e.g. a society or other partner) holds exclusive rights to this article under a publishing agreement with the author(s) or other rightsholder(s); author self-archiving of the accepted manuscript version of this article is solely governed by the terms of such publishing agreement and applicable law.

© The Author(s), under exclusive licence to Springer Nature Limited 2023

Methods

Experimental details of optical transient absorption spectroscopy

The output from the Ti:sapphire amplifier (Legend Elite HE+, Coherent Inc., 6 mJ, 45 fs, 790 nm, 1 kHz) was used to pump an optical-parametric amplification system (TOPAS-HE, Light Conversion Inc.). The signal (approximately 1,300 nm) and idler (approximately 1,900 nm) from the optical-parametric amplification system were mixed in a GaSe crystal (Eksma Optics Inc., z-cut, 0.5 mm thick) for difference-frequency generation, and the generated mid-infrared pulse was spectrally filtered by a bandpass filter that was centred at 4.00 μm (Thorlabs Inc., FB4000-500). For the 7 μm measurement, a different bandpass filter at 7.0 μm (Thorlabs Inc., FB7000-500) was used and the orientation of the GaSe crystal was adjusted for phase matching at 7 μm . A combination of wire-grid polarizers served to clean up the polarization of the mid-infrared pulse, while enabling continuous tuning of the laser intensity. The broadband visible pulse was produced by focusing the signal pulse on a 3 mm sapphire plate. The mid-infrared pump and the visible probe were linearly polarized in the same direction. The pump and probe pulses were focused onto a sample by a 150 mm ZnSe lens and by a 100 mm off-axis parabola, respectively, with a crossing angle of approximately 25°. The field strength of the mid-infrared pulse was estimated from the measured spot size (approximately 250 μm) and the pulse duration (approximately 200 fs), with the substrate effect included through the Fresnel factor of $2/(1+n_{\text{fs}})$, where $n_{\text{fs}} \approx 1.4$ is the refractive index of the fused-silica substrate⁴². The monolayer WS₂ was placed in an optical cryostat (ST-100, Lake Shore Cryotronics, Inc.) at a temperature of 77 K. The transmitted visible spectra were collected by a CaF₂ lens and directed into a fast-rate spectrometer (Ocean Insight Inc., Ocean-FX). The pump-on and pump-off spectra (I_{on} and I_{off}) were recorded on a single-shot basis at 1 kHz, and the $\Delta\text{OD} = -\log(I_{\text{on}}/I_{\text{off}})$ was obtained at controlled delay times. The detection sensitivity of 3×10^{-5} was achieved for the accumulation of 30,000 spectra (that is, 15,000 pump-on and pump-off spectra each). A monolayer WS₂ sample was exfoliated from a bulk single crystal (HQ graphene) on a passivated fused-silica substrate (100 μm thick, double-side polished, MTI corporation) by the gold-tape exfoliation method^{26,27}. The experimental linewidth of the A-exciton peak (full-width at half-maximum) was approximately 35 meV at 293 K, and approximately 15 meV at 77 K. Characterization of the sample quality, including the low-temperature photoluminescence measurements, has been presented in the literature²⁷.

2D-TDSE simulation

In the 2D-TDSE method, the Hamiltonian of the exciton wavepacket is given by

$$H(x, y, t) = -\frac{1}{2\mu} \frac{\partial^2}{\partial x^2} - \frac{1}{2\mu} \frac{\partial^2}{\partial y^2} - V(x, y) - \mathbf{E}(t) \cdot \mathbf{d}(x, y) - \frac{i\Gamma}{2}, \quad (2)$$

where μ is the reduced mass of an exciton, $V(x, y)$ is the model electron-hole potential, $\mathbf{E}(t)$ is the external laser field, \mathbf{d} is the dipole moment and Γ is the an imaginary potential to account for the finite lifetime of excitons. Atomic units are used in this section. As described in the main text, the reduced mass of the exciton is taken to be $\mu = 0.16 m_0$, as determined previously by density functional theory calculations³⁶. The free parameter of the screening length is chosen to be $r_0 = 50 \text{ \AA}$ to reproduce the experimental 1s–2p transition energy of 0.18 eV. The exciton binding energies reported for monolayer WS₂ range from 0.32 eV (ref. 24) to 0.7 eV (ref. 28), and the value obtained with these parameters, 0.42 eV, falls within this range. The imaginary potential of $\Gamma = 15 \text{ meV}$ is used, which yields a phenomenological $1/e$ dephasing time constant of 44 fs, to match the experimental linewidth of the 1s-exciton signal. The mid-infrared laser is approximated as a 75 fs Gaussian pulse with

a centre wavelength of 4 μm , and the visible laser pulse is approximated as a 1 fs Gaussian pulse with a centre wavelength of 600 nm. In the calculations, the laser fields are assumed to be polarized along the x direction. The exciton wavepacket is represented by the sinc-function discrete variable representation (sinc-DVR)⁴³ on 80×80 two-dimensional grids that span from -300 \AA to 300 \AA . A complex absorption potential is defined at the grid boundary to prevent reflection of the wavepacket, which also models strong-field ionization of the excitons. The time-dependent Schrödinger equation is solved numerically by using the fourth-order Runge–Kutta method at a step size of 31 as up to 500 fs. The absorption cross-section of the exciton wavepacket is calculated as

$$\sigma(\omega) \propto \omega \text{Im} \left[\frac{\tilde{d}(\omega)}{\tilde{E}(\omega)} \right], \quad (3)$$

where $\tilde{d}(\omega)$ and $\tilde{E}(\omega)$ are the Fourier-transformed optical dipole moment and laser electric field, respectively³⁷. The optical dipole moment $d(t)$ is considered proportional to the density of the wavepacket at $x, y = 0$, which is a common approach used to calculate absorption spectra of semiconducting nanomaterials^{44,45}. A constant energy shift is added to the absorption cross-section so that the position of the 1s-exciton signal matches with the experimentally measured value (2.07 eV). For the simulation results presented in Fig. 3, the absorption spectra are averaged over two mid-infrared pulses, a cosine pulse and a sine pulse, to take into account the randomized carrier-envelope phase of the experimental mid-infrared pulses.

1s–2p model simulation

In the 1s–2p model, the Hamiltonian of the exciton states is simplified as

$$H(t) = \begin{pmatrix} 0 & E(t)d_{g,1s} & 0 \\ E(t)d_{g,1s} & \epsilon_{1s} - i\Gamma/2 & E(t)d_{1s,2p} \\ 0 & E(t)d_{1s,2p} & \epsilon_{2p} - i\Gamma/2 \end{pmatrix}, \quad (4)$$

where ϵ_i and d_{ij} represent the energy and transition dipole moment, respectively. These state parameters are obtained from the effective model potential used in the 2D-TDSE method. The same parameters and methods as in the 2D-TDSE method are used for the laser field, exciton lifetime and time propagation. The optical dipole moment is obtained as

$$d(t) = \langle \Psi(t) | d | \Psi(t) \rangle, \quad (5)$$

where $\Psi_{(t)}$ is a column vector for the state coefficients and d is the transition dipole matrix. The absorption cross-section is calculated in the same way using equation (3).

Data availability

Source data are provided with this paper. All other data that support the plots within this paper and other findings of this study are available from the corresponding author upon reasonable request.

Code availability

The codes that support the findings of this study are available from the corresponding author upon reasonable request.

References

42. Higuchi, T., Heide, C., Ullmann, K., Weber, H. B. & Hommelhoff, P. Light-field-driven currents in graphene. *Nature* **550**, 224–228 (2017).
43. Colbert, D. T. & Miller, W. H. A novel discrete variable representation for quantum mechanical reactive scattering via the S-matrix Kohn method. *J. Chem. Phys.* **96**, 1982 (1992).

44. Glutsch, S., Chemla, D. S. & Bechstedt, F. Numerical calculation of the optical absorption in semiconductor quantum structures. *Phys. Rev. B* **54**, 11592 (1996).
45. Zhang, T. Y. & Zhao, W. Franz-Keldysh effect and dynamical Franz-Keldysh effect of cylindrical quantum wires. *Phys. Rev. B* **73**, 245337 (2006).

F.L., D.A.R., T.F.H. and S.G. supervised the project. V.T. performed supplementary calculations. All authors contributed to the preparation of the manuscript.

Competing interests

The authors declare no competing interests.

Additional information

Supplementary information The online version contains supplementary material available at <https://doi.org/10.1038/s41567-022-01849-9>.

Correspondence and requests for materials should be addressed to Yuki Kobayashi or Shambhu Ghimire.

Peer review information *Nature Physics* thanks the anonymous reviewers for their contribution to the peer review of this work.

Reprints and permissions information is available at www.nature.com/reprints.

Acknowledgements

We thank J. Shi and I. Franco for discussions. This work was primarily supported by the US Department of Energy, Office of Science, Basic Energy Sciences, Chemical Sciences, Geosciences, and Biosciences Division through the AMOS program. F.L. was supported by the Terman Fellowship and startup funds from the Department of Chemistry at Stanford University. Y.K. acknowledges support from the Urbanek-Chorodow Fellowship at Stanford University and C.H. acknowledges support from the W. M. Keck Foundation and an Alexander von Humboldt Research Fellowship.

Author contributions

Y.K. and C.H. performed the experiments. A.C.J. and F.L. fabricated the sample. Y.K. performed the simulations and analysed the results.